Biochemical and Biophysical Research Communications 828 (2026) 154068

Contents lists available at ScienceDirect

Biochemical and Biophysical Research Communications

journal homepage: www.elsevier.com/locate/ybbrc

Multiple comprehensive analyses identify that upregulation of Myomesin 2 suppresses cardiomyocyte proliferation

Shota Suzuki [a], Shota Tanaka [a], Yuriko Wada [a], Yusuke Kametani [a], Hibiki Sakai [a], Kosuke Nishinaka [a], Kaho Egawa [a], Yoshiaki Okada [b,c], Masanori Obana [a,d,e,f], Yasushi Fujio [a,c,d,*]

[a] Laboratory of Clinical Science and Biomedicine, Graduate School of Pharmaceutical Sciences, The University of Osaka, Suita City, Osaka, Japan
[b] Laboratory of Cardiovascular Science and Drug Discovery, Graduate School of Pharmaceutical Sciences, The University of Osaka, Suita City, Osaka, Japan
[c] Center of Infections Disease Education and Research, The University of Osaka, Suita City, Osaka, Japan
[d] Institute for Open and Transdisciplinary Research Initiatives, The University of Osaka, Suita City, Osaka, Japan
[e] Global Center for Medical Engineering and Informatics, The University of Osaka, Suita City, Osaka, Japan
[f] Radioisotope Research Center, Institute for Radiation Sciences, The University of Osaka, Suita City, Osaka, Japan

ARTICLE INFO

Keywords:
Cardiomyocytes
Cell proliferation
RNA-Seq
Single-cell analysis
Sarcomeres

ABSTRACT

Mammalian cardiomyocytes lose their proliferative capacity shortly after birth; however, molecular mechanisms that regulate cardiomyocyte proliferation remain to be fully elucidated. This study aimed to identify genes that regulate cardiomyocyte proliferation through multiple comprehensive analyses. RNA-sequencing analysis was performed using proliferating neonatal rat cardiomyocytes. We also retrieved and analyzed publicly available single-cell RNA-sequencing datasets from rat hearts on postnatal days 1 and 7. Pseudotime trajectory analysis identified a cardiomyocyte cluster undergoing cell cycle exit at postnatal day 7. Comparative gene expression analysis of this cluster between postnatal day 1 and day 7 identified *Myomesin 2* (*Myom2*) as a candidate for regulation of cardiomyocyte proliferation. Real time qRT-PCR analysis demonstrated that *Myom2* expression increased during cardiac maturation. Further, we investigated the effect of *Myom2* expression on cardiomyocyte proliferation. Immunofluorescence microscopic analysis revealed that adenoviral overexpression of *Myom2* significantly reduced the proportion of proliferating cardiomyocytes and promoted cardiomyocyte binucleation. Collectively, these findings indicate that postnatal induction of *Myom2* suppresses cardiomyocyte proliferation and promotes binucleation.

1. Introduction

Although adult mammalian cardiomyocytes (CMs) undergo turnover at a very low rate, the majority of CMs largely lose proliferative activities immediately after birth [1,2]. Previous studies have shown that postnatal day 1 mice could completely regenerate their hearts after apical resection or myocardial infarction, whereas postnatal day 7 mice could not [3,4]; however, molecular mechanisms underlying the regulation of CM proliferation remain to be fully elucidated.

The Fluorescent Ubiquitination-based Cell Cycle Indicator (FUCCI) system is the fluorescent probe that enables visualization of cell cycle progression [5]. The FUCCI system allows monitoring cell cycle in living cells without fixation [6,7]. To analyze gene expression profile, proliferating CMs were isolated using FUCCI system. The FUCCI system targets the DNA replication licensing factor Cdt1, a marker of the G1 phase, and its inhibitor Geminin, an S/G2/M phase marker. In this study, we used Geminin fused to mAG1 [5,7], known as Fucci-S/G2/M Green, which is stabilized and expressed during the S/G2/M phase [6], as CMs predominantly exit the cell cycle and remain in the G1 phase.

Notable alterations in myofibrils of CMs occur during cardiac growth [8]. The M-band is located in the middle of the sarcomere and serves to align myosin filaments with the A-bands. By linking myosin filaments, M-band reduces the longitudinal instability during sarcomere contraction [9]. *Myomesin 2* (*Myom2*) is a component of the M-band in sarcomere and is expressed in CMs and fast-twitch muscles [10]. The

* Corresponding author. Laboratory of Clinical Science and Biomedicine, Graduate School of Pharmaceutical Sciences, The University of Osaka, 1-6 Yamadaoka, Suita City, Osaka, 565-0871, Japan.
E-mail address: fujio@phs.osaka-u.ac.jp (Y. Fujio).

https://doi.org/10.1016/j.bbrc.2026.154068
Received 6 January 2026; Received in revised form 27 May 2026; Accepted 29 May 2026
Available online 29 May 2026

expression of *Myom2* increases from the neonatal to the adult stage in the heart [11,12], although its biological significance in cardiac maturation remains unclear.

In this study, to explore the genes responsible for the regulation of CM proliferation, we performed RNA-sequencing analysis of proliferating CMs using the FUCCI system. Additionally, we analyzed publicly available single-cell RNA-sequencing datasets. Integrated analysis revealed that the expression of *Myom2* expression was consistently low under proliferative conditions. Furthermore, adenoviral overexpression of *Myom2* suppressed CM proliferation and promoted binucleation. Collectively, these findings indicate that increased *Myom2* suppresses CM proliferation.

2. Materials and methods

2.1. Neonatal rat cardiomyocyte culture

All animal procedures were approved by the Animal Experimentation Committee of The University of Osaka and conducted in accordance with the Guide for the Care and Use of Laboratory Animals issued by the US National Research Council.

Neonatal rat cardiomyocytes (NRCMs) were isolated from 1–2-day-old Wistar rats of either sex [13]. Ventricular tissues were excised and enzymatically dissociated using 0.1% collagenase type IV (Sigma-Aldrich, C5138) and 0.1% trypsin (Gibco, 27250018). Cell suspensions were passed through a cell strainer (Falcon, 352360) and plated onto 10-cm culture dishes (Iwaki, 3020-100) for 90 min to minimize contamination by non-cardiomyocytes. Non-adherent cells were collected and maintained in Dulbecco's modified Eagle medium (DMEM; Sigma-Aldrich, D5796) supplemented with 10% fetal bovine serum (FBS; Gibco, A5256701).

For RNA-sequencing and proliferation assays, adenoviral transduction was carried out immediately after plating. After 24 h, culture medium was replaced with either serum-free medium or DMEM containing indicated concentration of FBS. In experiments using *Myom2*-expressing adenoviral vector, NRCMs were infected 24 h after plating and subsequently cultured for an additional 24 h in medium containing 10% FBS. For proliferation analyses, cells were maintained in medium supplemented with 1% FBS for a total duration of 72 h, with medium replacement every 24 h.

2.2. Adenoviral vectors

To generate the FUCCI-expressing adenoviral construct, insert sequence was obtained from the pFucci-S/G2/M Green Cloning Vector (MBL, AM-V9014 M) and subcloned into the pACCMVpLpA plasmid. Recombinant adenoviruses were generated in HEK293 cells through co-transfection with pJM17 to facilitate homologous recombination [14].

The adenoviral vector encoding *Myom2* was generated using the Adeno-X Adenoviral System 3 (CMV) (Clontech, 632269) according to the manufacturer's instructions. Viral particles were purified by $CsCl_2$ gradient ultracentrifugation, and viral titers were determined using the Adeno-X Rapid Titer Kit (Clontech, 632250).

The multiplicity of infection (MOI) used in each experiment was as follows: FUCCI, 2; GFP, 2; *Myom2*, 100; and β-gal, 100.

2.3. Flow cytometry

After 48 h of culture, NRCMs were detached using trypsin-EDTA solution containing 0.25% trypsin and 0.02% EDTA. Cells were resuspended in phosphate-buffered saline (PBS) supplemented with 1.5% FBS and filtered through a 70-μm cell strainer prior to analysis. Cell sorting and flow cytometric analyses were performed using FACS Aria II instrument and FACS DIVA software (BD Biosciences).

2.4. RNA-sequencing analysis

NRCMs were infected with adenoviral vectors expressing FUCCI or GFP at the time of plating. After 24 h, the culture medium was replaced with either 10% FBS-containing medium for the FUCCI group or serum-free medium for the GFP group, followed by an additional 24 h incubation. Cells were subsequently harvested and isolated by flow cytometric sorting.

Total RNA was extracted using the NucleoSpin RNA Plus XS kit (MACHEREY-NAGEL, 74990). Sequencing libraries were prepared using the TruSeq stranded mRNA sample preparation kit (Illumina, 20020594) and subjected to paired-end 100-bp sequencing on the Illumina NovaSeq 6000 platform.

Sequencing reads were aligned to the rat reference genome (Rn6) using TopHat (v2.0.13) in combination with Bowtie2 (v2.2.3) and SAMtools (v0.1.19). Transcript abundance was quantified as fragments per kilobase of exon per million mapped reads (FPKM) using Cufflinks (v2.2.1). Genes with low expression levels (average FPKM <1) were excluded prior to downstream analyses. Differentially expressed genes were identified using a threshold of >2-fold change and $p < 0.05$.

Differentially expressed genes in Fucci-S/G2/M Green-positive NRCMs were visualized using volcano plots generated with ggplot2 (v3.5.2). Heatmaps representing the top 30 upregulated and downregulated genes were generated using heatmaply (v1.6.0).

Gene Ontology (GO) and Kyoto Encyclopedia of Genes and Genomes (KEGG) pathway enrichment analyses of differentially expressed genes were conducted using ClusterProfiler (v4.14.6) [15]. Sequencing data have been deposited in the DDBJ BioProject database under accession number PRJDB39946.

2.5. Single-cell RNA-sequencing analysis

Publicly available single-cell RNA-sequencing datasets (GSE182422) [16] were analyzed using Seurat (v5.3.0) [17]. For the P1 rat dataset, cells with 200–6000 detected genes and mitochondrial gene content below 60% were retained. For the P7 rat dataset, filtering criteria included 200–5500 detected genes and mitochondrial gene content below 60%. Following quality control filtering, 7844 cells from P1 rats and 8203 cells from P7 rats were included in subsequent analyses.

Each dataset was normalized using the NormalizeData function with the "LogNormalize" method and a scale factor of 10,000. The top 2000 highly variable genes were identified using the FindVariableFeatures function and used for integration anchor generation. Genes exhibiting shared variation across datasets were selected using SelectIntegrationFeatures function. Dataset integration was subsequently performed using IntegrateData, followed by data scaling with ScaleData.

Cell clustering was conducted using the FindNeighbors and FindClusters functions. Dimensionality reduction and data visualization were performed using principal component analysis (PCA) and Uniform Manifold Approximation and Projection (UMAP). Pseudotime trajectory analysis was conducted using Monocle3 (v1.4.26) [18].

2.6. Isolation of cardiomyocytes from postnatal day 7 rats

Postnatal day 7 rats were anesthetized with isoflurane (Wako, 099-06571), and hearts were excised immediately after euthanasia. Excised hearts were cannulated and perfused retrogradely perfused for 3 min with perfusion buffer containing 120.4 mM NaCl, 14.7 mM KCl, 0.6 mM $NaHCO_3$, 0.6 mM KH_2PO_4, 0.4 mM Na_2HPO_4, 1.2 mM $MgSO_4$, 10 mM HEPES, 30 mM taurine, 10 mM 2,3-butanedione monoxime, and 5.5 mM glucose.

Enzymatic digestion was subsequently performed using digestion buffer composed of perfusion buffer supplemented with 12.5 μM $CaCl_2$, 0.32 mg/mL collagenase B (Roche, 11088815001), 0.24 mg/mL collagenase D (Roche, 11088866001), and 0.04 mg/mL protease type XIV (Sigma, P5147). After 15 min of perfusion, hearts were transferred to

stop buffer consisting of perfusion buffer supplemented with 12.5 μM $CaCl_2$ and 5% FBS, followed by gentle mechanical dissociation using pipetting and tissue disruption using fine forceps.

Cell suspensions were filtered through a 100-μm cell strainer and subjected to gravity sedimentation for 20 min to enrich CMs. Following removal of the supernatant, cell pellets were resuspended in PC buffer consisting of perfusion buffer supplemented with 12.5 μM $CaCl_2$ and allowed to sediment for an additional 20 min. After the second sedimentation step, the supernatant was discarded, and the pellet was resuspended again in PC buffer. Purified CMs were then collected by centrifugation at 200 × *g* for 3 min and used for quantitative RT-PCR analysis.

2.7. Quantitative RT-PCR

Total RNA was isolated from cultured NRCMs, CMs obtained from P7 rats, or mouse heart tissue using QIAzol Lysis Reagent (QIAGEN, 79306), as described in a previous study [19]. First-strand cDNA synthesis was performed from 1 μg of total RNA using ReverTra Ace (Toyobo, TRT-101) and oligo(dT) primers (Thermo, 18418020).

Quantitative PCR was conducted using FAST SYBR Green Master Mix (Applied Biosystems, 4385612) on a StepOne Real-Time PCR System (Applied Biosystems). Primer sequences used in this study are listed below.

Primers for rat genes.

Myom2 forward, 5′-CTCCTCATCTTTCTGGGAATATCC-3'; reverse, 5′-ATGATTGACTGGACGCTTGC-3'

Tcea3 forward, 5′-AGAAGAGCTGCTGAGGATCG-3'; reverse, 5′-ATCCTGGTGGTCTGTAGCAG-3'

Scx forward, 5′-CAACCAGAGAAAGTTGAGCAAAG-3'; reverse, 5′-TCTTCAGTGGCTTCCACCTTC-3'

Ccng2 forward, 5′-TGGAGGCTACCCCAGAGAATG-3'; reverse, 5′-AGGACAGGTGTTTGGGCTTC-3'

Bdh2 forward, 5′-AGGTGCATGTTTTTGGATTGC-3'; reverse, 5′-CTCTTGCGAAAGCTAAAGCAG-3'

B2m forward, 5′- TGACCGTGATCTTTCTGGTGC-3'; reverse, 5′-AAGTTGGGCTTCCCATTCTCC-3'

Primers for mouse genes.

Myom2 forward, 5′-AACACTCAAGATGTCCCTGGTC-3'; reverse, 5′-TCTGACTGGAAGCTCTCTTCG-3'

GAPDH forward 5′-CATCACCATCTTCCAGGAGCG-3'; reverse, 5′-GAGGGGCCATCCACAGTCTTC-3'

2.8. Immunoblot analysis

Immunoblot analysis was performed as described in a previous study [20]. Proteins extracted from cultured NRCMs or rat heart tissues were separated by SDS-PAGE and transferred onto polyvinylidene difluoride membranes (Merck Millipore, IPVH00010). Membranes were blocked with 5% bovine serum albumin (Nacalai Tesque, 0186007) for 1 h and incubated overnight at 4 °C with primary antibodies. After washing, membranes were incubated with HRP-conjugated secondary antibodies for 1 h at room temperature.

Protein bands were visualized using ECL Western Blotting Substrate (Promega, W1001) and detected with an ImageQuant LAS 4010 imaging system (Cytiva). Band intensities were quantified using ImageJ software. Antibodies used in this study are listed in Supplemental Table S1.

2.9. Immunofluorescence microscopy

Immunofluorescence microscopic analyses were performed as described previously [21]. Specifically, cells were fixed with 4% paraformaldehyde (Nacalai Tesque, 09154) for 15 min after washing with PBS. Following permeabilization with 0.1% Triton X-100 in PBS, samples were incubated overnight at 4 °C with primary antibodies. Alexa Fluor 488- or Alexa Fluor 546-conjugated secondary antibodies were subsequently applied for 1 h at room temperature. Nuclei were counterstained with DAPI.

Fluorescence images were acquired using a CV8000 fluorescence microscope (Yokogawa Electric). Nine independent fields were analyzed for each well. The numbers of total CMs and Ki-67$^+$, pHH3$^+$, or Aurora B$^+$ CMs were quantified. Sarcomere organization and cell surface area were evaluated by an investigator blinded to the experimental conditions. Antibodies used in this study are listed in Supplemental Table S2.

2.10. siRNA transfection

Twenty-four hours after plating, NRCMs were transfected with siRNA using Lipofectamine RNAiMAX Transfection Reagent (Invitrogen, 13778-150) according to the manufacturer's instructions. After 24 h of transfection, the culture medium was replaced with serum-free medium.

The siRNA sequences used in this study were as follows:

Cont (Merck, SIC-10NMOL): proprietary sequence provided by the manufacturer.

Myom2 (Merck, SASI_Rn02_0034729)

Forward, 5′-GAUAAAGAAUCCCACAAUU-3'

Reverse, 5′-AAUUGUGGGAUUCUUUAUC-3'

2.11. Statistical analysis

Data are presented as mean ± standard deviation (SD). Comparisons between two groups were performed using Student's *t*-test or Welch's *t*-test, as appropriate. Multiple-group comparisons were analyzed by one-way ANOVA followed by the Tukey–Kramer post hoc test. Statistical significance was defined as $p < 0.05$.

3. Results

3.1. RNA-sequencing analysis of proliferating cardiomyocytes isolated using the FUCCI system

To explore the regulatory genes involved in CM proliferation, we performed RNA-sequencing analysis of proliferating CMs. To isolate proliferating cells, we used adenoviral vector expressing Fucci-S/G2/M Green. To enhance the efficiency of proliferating CM isolation, Fucci-S/G2/M Green-expressing CMs were cultured in medium supplemented with 10% FBS. Flow cytometry analysis confirmed that serum stimulation increased the proportion of Fucci-S/G2/M Green-positive CMs (Supplementary Fig. S1A–C). As control, NRCMs were infected with GFP-expressing adenoviral vector and cultured in serum-free medium. Immunofluorescence microscopic analysis confirmed that adenoviral labeling was selective for α-actinin-positive CMs (Supplementary Fig. S2A–D). After labeling proliferating cells using adenoviral vectors, the labeled cells were sorted by flow cytometry (Supplementary Fig. S3A and B) and then subjected to RNA-sequencing analysis (Fig. 1A). Genes with > 2-fold change between GFP-positive NRCMs and Fucci-S/G2/M Green-positive NRCMs with a *p*-value <0.05 were defined as differentially expressed genes. In Fucci-S/G2/M Green-positive NRCMs, 181 genes were upregulated and 137 genes were downregulated (Fig. 1B). As expected, cell cycle-related genes, such as *Plk1*, *Ccnb1*, and *Aurka*, were among the upregulated genes (Fig. 1C), whereas fatty acid metabolism-related genes, including *Klf15* [22] and *Scd1* [23], were among the downregulated genes (Fig. 1D). These findings are consistent with previous reports indicating that the metabolic shift from glycolysis to fatty acid oxidation contributes to the loss of proliferative capacity in CMs [8]. GO analysis (Fig. 1E) and KEGG pathway analysis (Fig. 1F) revealed significant enrichment of cell cycle-related terms. These findings indicate that proliferating CMs were successfully isolated using Fucci-S/G2/M Green.

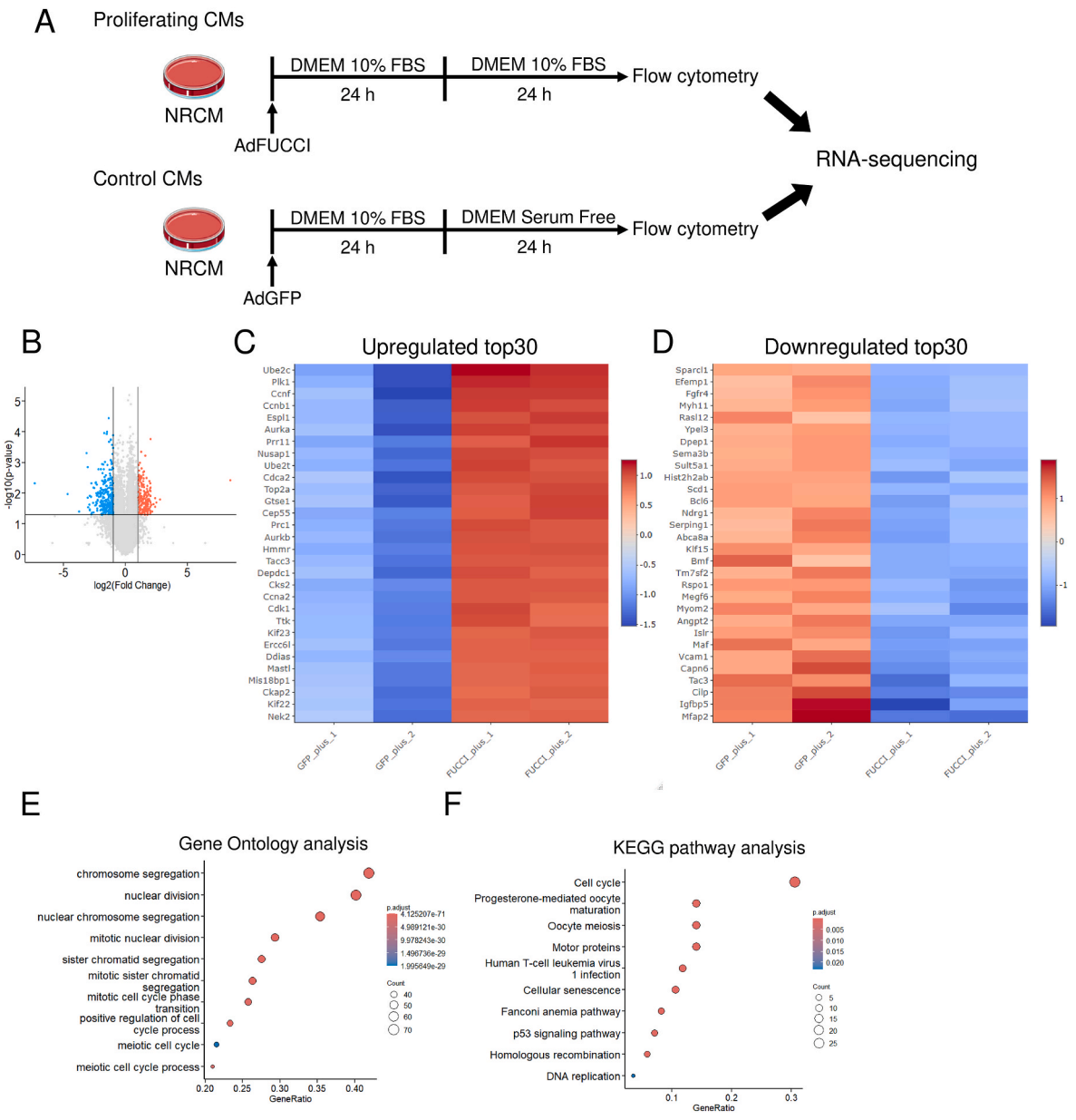

Fig. 1. RNA-sequencing analysis of Fucci-S/G2/M Green-positive, proliferating NRCMs. (A) Schematic diagram of isolating proliferating NRCMs. NRCMs were infected with an adenoviral vector expressing Fucci-S/G2/M Green at the time of seeding. After culture with FBS-containing Dulbecco's modified Eagle medium, labeled NRCMs were isolated by flow cytometry. Control cells, infected with an adenoviral vector expressing GFP, were cultured in serum-free medium, followed by isolation using flow cytometric sorting. Total RNA was extracted, and RNA-sequencing analysis was performed ($n = 2$ for each group). Images provided by Servier Medical Art (https://smart.servier.com), licensed under CC BY 4.0 (https://creativecommons.org/licenses/by/4.0/). (B) Volcano plot shows differentially expressed genes. Red dots indicate upregulated genes, and blue dots indicate downregulated genes in proliferating NRCMs. (>2-fold change between FUCCI and control, $p < 0.05$) (C, D) Heatmaps for the top 30 upregulated genes (C) and for the top 30 downregulated genes (D). (E) Gene Ontology (GO) analysis of upregulated genes in proliferating CMs revealed an enrichment in GO terms involved in cell cycle. (F) Kyoto Encyclopedia of Genes and Genomes (KEGG) pathway analysis of the genes upregulated in proliferating CMs also revealed a significant enrichment of cell cycle-related pathways. (For interpretation of the references to colour in this figure legend, the reader is referred to the Web version of this article.)

3.2. Cell cycle exit of cardiomyocytes analyzed by single-cell RNA-sequencing data

Mammalian CMs lose their proliferative capacity within seven days after birth [3]. To investigate gene expression changes associated with this process, we compared postnatal day 1 (P1) and day 7 (P7) CMs using single-cell RNA-sequencing data of P1 and P7 from the Gene Expression Omnibus database (GSE182422) [16]. Single-cell RNA-sequencing data were analyzed using Seurat [17]. Uniform Manifold Approximation and Projection (UMAP) analysis identified 22 clusters in P1 and P7 hearts (Fig. 2A). Clusters 0, 2, 3, 8, 9, 12, 16 and 20 were identified as CMs based on high expression of CM marker genes, such as *Myh6* and *Cox6a2* (Fig. 2B and C). After extracting CM clusters and re-clustering, we detected 11 CM subclusters (Fig. 2D). CellCycleScoring function revealed that cluster 5 predominantly consisted of S-phase cells, whereas cluster 6 consisted of G2/M-phase cells (Fig. 2E). Next, we conducted pseudotime trajectory analysis using Monocle3 (Fig. 2F) [18]. In P1 CMs, trajectory from G1 phase to S/G2/M phases was detected (Fig. 2G). In contrast, in P7 CMs, the trajectory was interrupted at cluster 5, suggesting arrest at the G1/S-phase transition (Fig. 2H). To characterize this arrested population, we compared gene expression in cluster 5 between P1 and P7 CMs by pseudobulk analysis. A total of 335

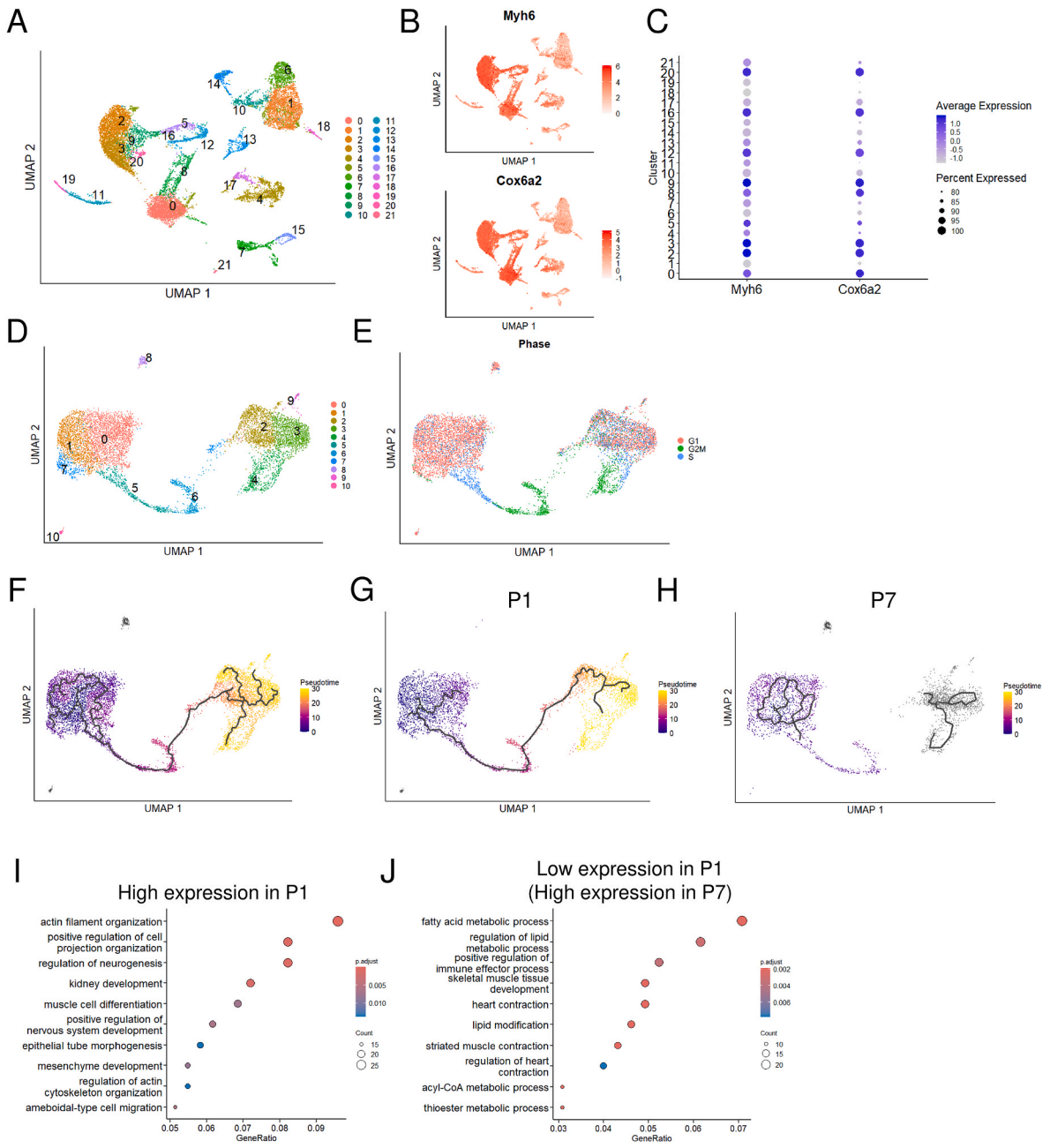

Fig. 2. Cell cycle exit of cardiomyocytes analyzed by single-cell RNA-sequencing data. (A) Uniform Manifold Approximation and Projection (UMAP) plot identifies 22 clusters in postnatal day 1 (P1) and postnatal day 7 (P7) rat hearts. (B) Feature plots showing the expression of cardiomyocyte markers *Myh6* and *Cox6a2*. (C) Dot plots showing the expression of *Myh6* and *Cox6a2* in each cluster. (D) UMAP plot indicates 11 cardiomyocyte clusters in P1 and P7 hearts. (E) UMAP plot showing cell cycle stages. (F–H) Pseudotime trajectory analysis was performed using Monocle3. (F) UMAP plots showing pseudotime trajectories in P1 and P7 hearts. (G) UMAP plot indicating the trajectory in the P1 heart. (H) UMAP plot indicating the trajectory in P7 heart, in which the trajectory was interrupted at cluster 5. (I, J) For cluster 5, pseudobulk analysis was performed to compare P1 and P7 cardiomyocytes. GO analysis was conducted using highly expressed genes in P1 (I) and P7 (J) cells.

genes were highly expressed in P1 CMs, whereas 389 genes were expressed at lower levels in P1 CMs. GO analysis revealed enrichment of actin filament organization among genes highly expressed in P1 CMs (Fig. 2I), whereas genes with low expression in P1 CMs and highly expressed in P7 CMs were enriched in processed related to fatty acid metabolism and heart contraction (Fig. 2J).

3.3. *Myom2 is identified as a candidate inhibitor of CM proliferation*

To identify regulatory genes involved in CM proliferation, we integrated the results of two comprehensive analyses (Fig. 3A and B). One gene, *Tuba1c*, was consistently highly expressed (Fig. 3A), whereas five genes, including *Myom2*, *Tcea3*, *Scx*, *Ccng2*, and *Bdh2*, were expressed at low levels (Fig. 3B). Given the established role of tubulin in mitotic spindle formation during the cell cycle, we focused on the down-regulated genes as potential regulators of CM proliferation. Among the five genes, *Myom2* expression was markedly decreased in proliferating NRCMs (−4.024-fold, $p = 0.034$) (Fig. 3C–Supplemental Table S3). We further examined the expression of these genes in P7 CMs and NRCMs cultured with or without serum stimulation by qRT-PCR analysis. *Myom2* mRNA expression was decreased in serum-stimulated NRCMs and enhanced in P7 CMs, whereas the other four genes did not exhibit

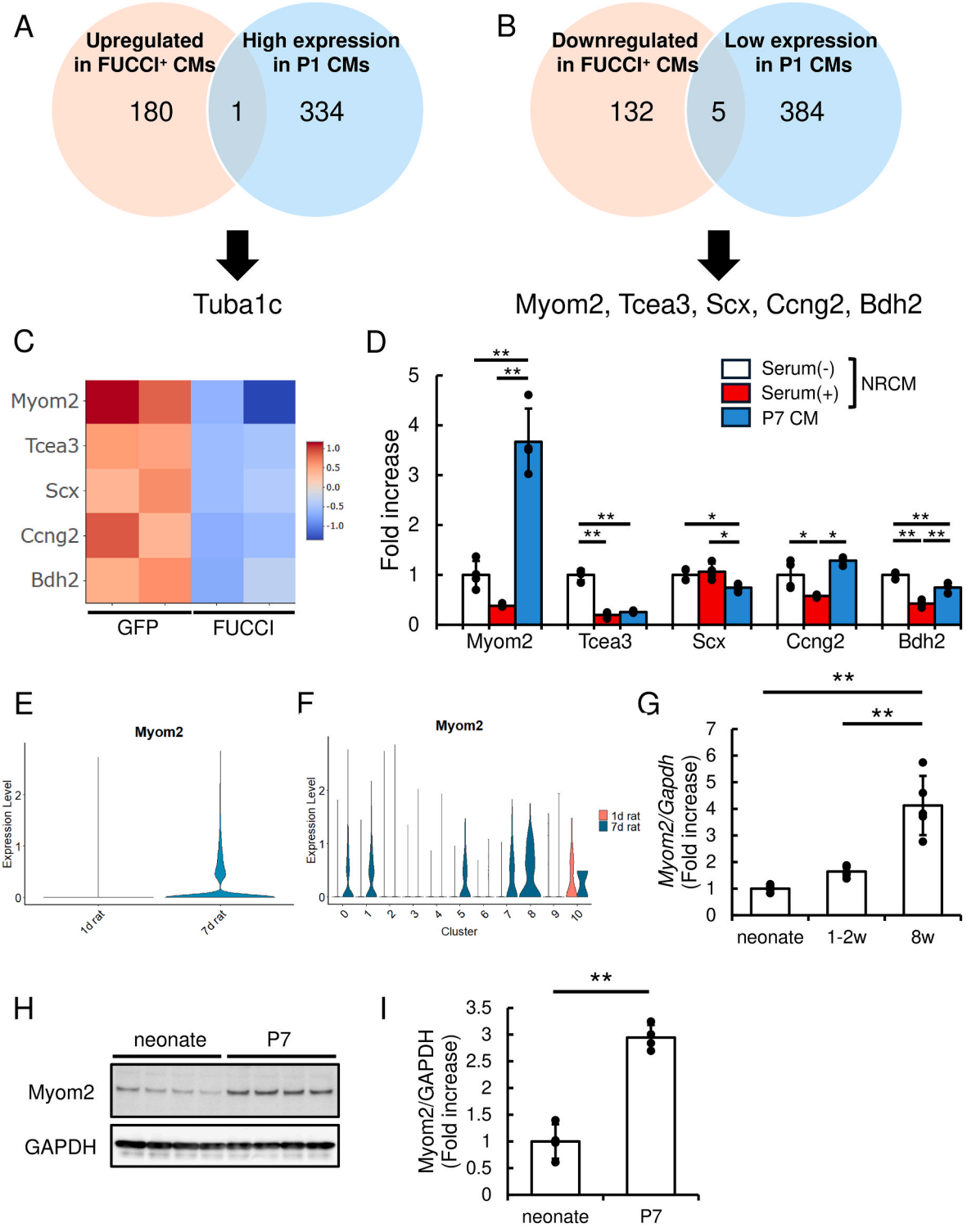

Fig. 3. Identification of Myom2 as a candidate inhibitor of CM proliferation by integrated analysis. (A, B) Venn diagrams showing genes consistently expressed at high (A) or low (B) levels in RNA-sequencing and single-cell RNA-sequencing analyses. (C) Heatmap showing expression of genes downregulated in RNA-sequencing analysis of proliferating CMs. (D) NRCMs were cultured in the medium with or without serum stimulation. Postnatal day 7 (P7) cardiomyocytes were isolated using the Langendorff method. The mRNA expression of *Myom2*, *Tcea3*, *Scx*, *Ccng2*, and *Bdh2* was quantified by qRT-PCR and normalized to *B2m* expression. Gene expression levels are presented as fold change relative to that of the serum (−) group. Data are shown as mean ± SD. $*p < 0.05$, $**p < 0.01$ ($n = 4$) by one-way ANOVA followed by Tukey–Kramer test. (E, F) Violin plots showing *Myom2* expression in single-cell RNA-sequencing analysis. (G) The mRNA expression of *Myom2* in mouse hearts was quantified by qRT-PCR and normalized to that of *Gapdh*. Data are shown as mean ± SD of fold change. $**p < 0.01$ ($n = 5$) by one-way ANOVA followed by Tukey–-Kramer test. (H, I) Immunoblot analysis was performed using anti-*Myom2* and anti-GAPDH antibodies. (H) Representative immunoblot images. (I) Quantitative analysis of *Myom2* expression. Data are shown as mean ± SD of fold change. $**p < 0.01$ ($n = 4$) by unpaired two-tailed Student's *t*-test.

similar expression patterns (Fig. 3D). Single-cell RNA-sequencing analysis demonstrated that *Myom2* was highly expressed in P7 CMs including cluster 5 (Fig. 3E and F). Consistent with previous studies reporting that *Myom2* expression increases from the neonatal to the adult stage [11,12], both *Myom2* mRNA and protein expression increased during cardiac maturation (Fig. 3G–I). Considering that mature CMs lose proliferative capacity [8], these findings suggest that *Myom2* upregulation may contribute to suppression of CM proliferation.

3.4. *Myom2* overexpression suppresses cardiomyocyte proliferation

To investigate whether the overexpression of *Myom2* inhibits CM proliferation, we generated an adenoviral vector expressing *Myom2* (AdMyom2). NRCMs were infected with the adenoviral vector at 100 MOI. Immunoblot analysis showed that adenoviral transduction increased *Myom2* protein expression (Fig. 4A and B).

Next, we evaluated the effects of *Myom2* overexpression on CM proliferation using an adenoviral vector β-galactosidase vector (Adβ-gal) as control. Immunofluorescence microscopic analyses using antibodies, including anti-Ki-67, anti-phospho-histone H3 (pHH3), and anti-Aurora kinase B (Aurora B), revealed that *Myom2* overexpression significantly decreased the proportions of Ki-67$^+$ CMs (Fig. 4C and D), pHH3$^+$ CMs (Fig. 4E and F), and Aurora B$^+$ CMs (Fig. 4G and H). CM binucleation is a characteristic of differentiated CMs with limited proliferative capacity in mice [24]. The overexpression of Myom2 increased the proportion of binucleated CMs (Fig. 4I).

Finally, as *Myom2* has been reported as a marker of CM maturation [12], we investigated whether *Myom2* influences CM maturation. Immunofluorescence microscopic analysis revealed that *Myom2* overexpression increased the proportion of NRCMs with organized sarcomeres (Supplementary Fig. S4A and B). Collectively, these findings suggest that *Myom2* upregulation suppresses CM proliferation and stabilizes sarcomere assembly, consistent with CM maturation.

4. Discussion

In this study, we analyzed the gene expression profile of proliferating NRCMs using the FUCCI system. We also analyzed the single-cell RNA-sequencing data of P1 and P7 rat hearts. By integrating these two results, we found that the expression of five genes was consistently low in proliferating CMs. Among them, the expression of *Myom2* was downregulated in serum-stimulated NRCMs but increased in P7 CMs; therefore, we focused on *Myom2*. The adenoviral overexpression of Myom2 suppressed proliferation of NRCMs and induced binucleation. These findings indicate that increased *Myom2* expression inhibits CM proliferation.

Although stimulation of CM proliferation represents a promising strategy for cardiac regeneration, the mechanisms underlying regulation of CM proliferation remain to be fully elucidated owing to the difficulty in obtaining purified CMs. Non-cardiac cells, which exhibit high proliferative activity, are contaminated in CM fraction during CM isolation, which can compromise analytical accuracy, particularly in studies focused on CM proliferation. Among cardiac cells, CMs account for approximately 30% of total cells, whereas the remaining 70% are non-CMs [25]. Although primary CM culture can enrich CMs to some extent, the low purity of primary CMs remains a significant challenge [26]. In this study, we utilized an adenoviral vector-based strategy combined with flow cytometry for the isolation of proliferating CMs. Regarding gene delivery using adenoviral vectors, the expression level of the viral binding proteins coxsackie and adenovirus receptor (CAR) determines the specificity and efficiency of delivery [27]. Importantly, CAR is strongly expressed in neonatal CMs [28]. Consistent with this, immunofluorescence microscopic analysis revealed that gene delivery by adenoviral vectors expressing GFP or Fucci-S/G2/M Green exhibited high selectivity of over 95% for CMs (Supplementary Fig. S2A–D). This implies that adenoviral labelling of CMs may be an effective approach for purification of primary cultured CMs.

Our single-cell analysis identified cell cycle-arrested CMs in cluster 5. In this cluster, genes associated with actin filament organization were enriched in P1 CMs, consistent with the previous findings showing that changes in the actin cytoskeleton, including sarcomere disassembly, occur during CM proliferation [29,30]. Moreover, fatty acid metabolic processes were significantly enriched in P7 CMs. Additionally, KEGG pathway analysis revealed enrichment of the PPAR signaling pathway, a key regulator of fatty acid metabolism [31], in P7 cells (Supplementary Fig. S5). Taken together, these findings suggest the P7 CMs in cluster 5, which are undergoing cell cycle exit, exhibit characteristics of mature CMs, including enhanced fatty acid oxidation and loss of actin filament dynamics.

In this study, adenoviral overexpression of *Myom2* reduced the proportion of Ki-67-, pHH3-, or Aurora B-positive CMs, indicating that upregulation of *Myom2* suppresses CM proliferation. However, the mechanisms by which *Myom2* regulates proliferation remain unclear. Sarcomere constitutes a large volume of CM cytoplasm and can physically interfere with mitosis and cytokinesis [32]. Sarcomere disassembly is an essential step in CM proliferation [33], called “dedifferentiation”. Because *Myom2* is a component of the M-band and contributes to sarcomere structural stability, it may inhibit sarcomere disassembly during mitosis or cytokinesis. Consistent with this, *Myom2* overexpression promotes sarcomere assembly of NRCMs (Supplementary Fig. S4A and B). Therefore, upregulation of *Myom2* may suppress CM proliferation by stabilizing sarcomere structure.

The Myomesin family consists of three members: *Myom*1, *Myom*2, and *Myom*3. *Myom*1 is broadly expressed in muscle tissues, whereas *Myom2* and *Myom3* exhibit tissue-specific expression patterns [10], suggesting that the expression of the Myomesin family members is differentially regulated. Embryonic heart (EH)-myomesin, a splice variant of *Myom*1, is expressed in embryonic CMs, whose M-bands are not clear. Around birth, the expression of EH-myomesin is downregulated, whereas *Myom2* expression is upregulated [9]. Regarding regulation of *Myom2* expression, the transcription factor myocyte enhancer factor 2c (Mef2c) binds to the *Myom2* promoter and regulates its expression [34]. Previously, we reported that RUNX family transcription factor 1 (*Runx1*) promotes CM juvenilization and proliferation [21]. *Runx1* is widely used as a marker of CM dedifferentiation [35–37]. Interestingly, RNA-sequencing data from our previous study (PRJDB16862) showed that *Runx1* overexpression significantly decreased the expression of *Myom2* (−7.258-fold, $p = 0.059$E-7)). *Runx1* deficiency in skeletal muscle cells and myoblasts has been reported to increase *Mef2c* expression [38,39]. These findings suggest that *Runx1* may negatively regulate *Myom2* expression through suppression of *Mef2c* expression.

Myom2 overexpression suppressed CM proliferation, whereas knockdown of *Myom2* unexpectedly reduced the proportion of Ki-67-positive NRCMs (Supplementary Fig. S6A–D). Notably, *Myom2* knockdown markedly disrupted sarcomere organization and induced cardiomyocyte shrinkage (Supplementary Fig. S6E and F). In addition, siRNA-mediated *Myom2* knockdown, but not *Myom2* overexpression, significantly increased the number of condensed nuclei in CMs (Supplementary Fig. S6G–I), suggesting that impaired cellular homeostasis or structural integrity may have indirectly influenced proliferative activity. Further studies are therefore required to distinguish direct cell cycle regulatory functions of *Myom2* from secondary effects caused by sarcomere disorganization. Another possibility is that the physiological roles of *Myom2* may depend on its intracellular localization and expression level. A recent study demonstrated that *Myom2* localizes to the nuclear envelope in human induced pluripotent stem cell-derived CMs when expressed at low levels [40]. We also observed perinuclear

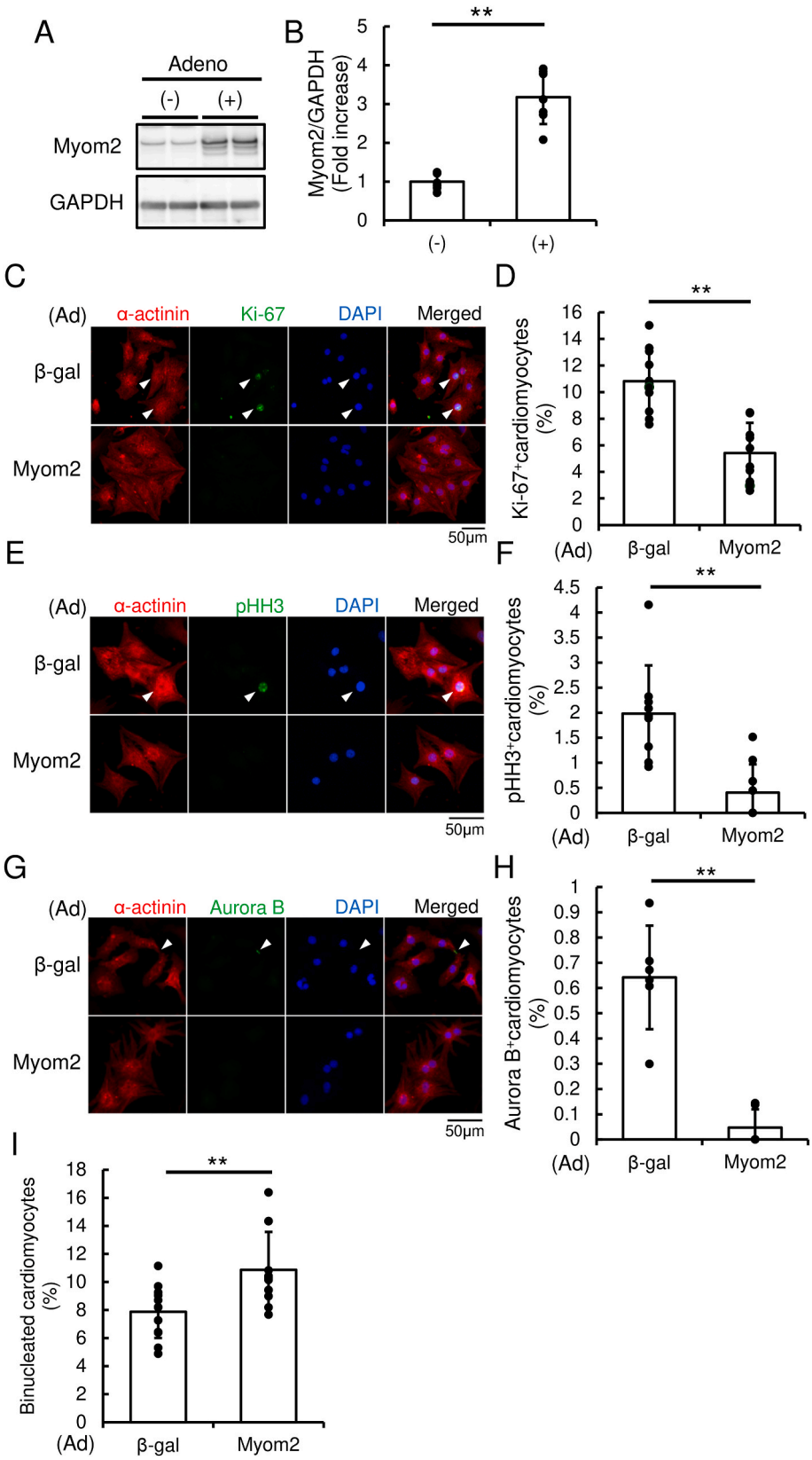

(caption on next page)

Fig. 4. Myom2 overexpression suppresses NRCM proliferation. (A, B) NRCMs were infected with adenoviral vector expressing *Myom2* at 100 MOI. Immunoblot analysis was performed using anti-*Myom2* and anti-GAPDH antibodies. (A) Representative immunoblot images. (B) Quantitative analysis of *Myom2* expression. Data are shown as mean ± SD of fold change. $^{**}p < 0.01$ ($n = 8$ for (−), $n = 7$ for (+)) by unpaired two-tailed Welch's *t*-test. (C–I) NRCMs were infected with adenoviral vector expressing *Myom2* or β-galactosidase (β-gal) as control at 100 MOI. (C, D) NRCMs were stained with anti-sarcomeric α-actinin and anti-Ki-67 antibodies. Nuclei were counterstained with DAPI. (C) Representative immunofluorescence images. Arrowheads indicate Ki-67$^+$ α-actinin$^+$ cells. (D) Quantification of the percentage of α-actinin$^+$ Ki-67$^+$ cells among total α-actinin$^+$ cells. Data are shown as mean ± SD. $^{**}p < 0.01$ ($n = 12$) by unpaired two-tailed Student's *t*-test. (E, F) NRCMs were stained with anti-sarcomeric α-actinin and anti-pHH3 antibodies. Nuclei were counterstained with DAPI. (E) Representative immunofluorescence images. Arrowhead indicates pHH3$^+$ α-actinin$^+$ cell. (F) Quantification of the percentage of α-actinin$^+$ pHH3$^+$ cells per α-actinin$^+$ cells. Data are shown as mean ± SD. $^{**}p < 0.01$ ($n = 9$) by unpaired two-tailed Student's *t*-test. (G, H) NRCMs were stained with anti-sarcomeric α-actinin and anti-Aurora B antibodies. Nuclei were counterstained with DAPI. (G) Representative immunofluorescence images. Arrowhead indicates Aurora B$^+$ α-actinin$^+$ cells. (H) Quantification of the percentage of α-actinin$^+$ Aurora B$^+$ cells among total α-actinin$^+$ cells. Data are shown as mean ± SD. $^{**}p < 0.01$ ($n = 6$) by unpaired two-tailed Welch's *t*-test. (I) Quantification of the percentage of binucleated cardiomyocytes. Data are shown as mean ± SD. $^{**}p < 0.01$ ($n = 12$) by unpaired two-tailed Student's *t*-test.

localization of *Myom2* in NRCMs (data not shown). Because the nuclear envelope has been implicated in the regulation of CM proliferation [41], *Myom2* may exert distinct functions depending on its abundance and subcellular localization, potentially supporting proliferation through nuclear envelope-associated mechanisms at low expression levels while suppressing proliferation through sarcomeric functions at higher expression levels.

In conclusion, we identified that increased *Myom2* expression suppresses CM proliferation based on RNA-sequencing analysis using the FUCCI system and single-cell RNA-sequencing analysis. Our data provide novel insights into the molecular mechanisms underlying the regulation of CM proliferation.

Ethics statement

Animal study protocols were approved by the Ethics Committee of The University of Osaka and Institutional Animal Care (Approval number: Douyaku, R03-16-8, approval date: December 15, 2021). Genetic modification experiments were conducted in accordance with the regulations for genetic modification experiments at The University of Osaka (Approval number: 04809, approval date: November 22, 2021).

Grants

This study was fully or partially supported by the MEXT/JSPS KAKENHI Grant 18K19545 and 25K02446 (Y.F.), Grant-in-Aid for Japan Society for the Promotion of Science Research Fellowships for Young Scientists 25KJ1784 (S.S.), and AMED (JP25ama121052 and JP25ama121054).

CRediT authorship contribution statement

Shota Suzuki: Conceptualization, Data curation, Investigation, Visualization, Writing – original draft, Writing – review & editing. **Shota Tanaka:** Conceptualization, Writing – review & editing. **Yuriko Wada:** Data curation, Formal analysis. **Yusuke Kametani:** Data curation, Writing – review & editing. **Hibiki Sakai:** Investigation. **Kosuke Nishinaka:** Data curation, Writing – review & editing. **Kaho Egawa:** Data curation, Writing – review & editing. **Yoshiaki Okada:** Writing – review & editing. **Masanori Obana:** Conceptualization, Writing – review & editing. **Yasushi Fujio:** Conceptualization, Funding acquisition, Project administration, Supervision, Writing – review & editing.

Declaration of competing interest

The authors declare that they have no known competing financial interests or personal relationships that could have appeared to influence the work reported in this paper.

Acknowledgements

We thank Prof. Hiroyuki Mizuguchi (The University of Osaka) and Prof. Fuminori Sakurai (Kindai University) for providing the adenoviral vector expressing GFP.

We also thank Reiko Kizaki (The University of Osaka) for her excellent administrative work.

Appendix A. Supplementary data

Supplementary data to this article can be found online at https://doi.org/10.1016/j.bbrc.2026.154068.

Data availability

Data supporting the findings of this study are available from the corresponding author, Y.F., upon reasonable request.

References

[1] O. Bergmann, R.D. Bhardwaj, S. Bernard, S. Zdunek, F. Barnabé-Heider, S. Walsh, et al., Evidence for cardiomyocyte renewal in humans, Science (New York, N.Y.) 324 (5923) (2009) 98–102, https://doi.org/10.1126/science.1164680.
[2] O. Bergmann, S. Zdunek, A. Felker, M. Salehpour, K. Alkass, S. Bernard, et al., Dynamics of cell generation and turnover in the human heart, Cell 161 (7) (2015) 1566–1575, https://doi.org/10.1016/j.cell.2015.05.026.
[3] E.R. Porrello, A.I. Mahmoud, E. Simpson, J.A. Hill, J.A. Richardson, E.N. Olson, et al., Transient regenerative potential of the neonatal mouse heart, Science (New York, N.Y.) 331 (6020) (2011) 1078–1080, https://doi.org/10.1126/science.1200708.
[4] E.R. Porrello, A.I. Mahmoud, E. Simpson, B.A. Johnson, D. Grinsfelder, D. Canseco, et al., Regulation of neonatal and adult mammalian heart regeneration by the miR-15 family, Proc. Natl. Acad. Sci. U. S. A 110 (1) (2013) 187–192, https://doi.org/10.1073/pnas.1208863110.
[5] A. Sakaue-Sawano, H. Kurokawa, T. Morimura, A. Hanyu, H. Hama, H. Osawa, et al., Visualizing spatiotemporal dynamics of multicellular cell-cycle progression, Cell 132 (3) (2008) 487–498, https://doi.org/10.1016/j.cell.2007.12.033.
[6] L. Fischer, I. Thievessen, FUCCI reporter gene-based cell cycle analysis, Methods in molecular biology (Clifton, NJ) 2644 (2023) 371–385, https://doi.org/10.1007/978-1-0716-3052-5_24.
[7] N. Zielke, B.A. Edgar, FUCCI sensors: powerful new tools for analysis of cell proliferation, Wiley Interdiscip. Rev.: Dev. Biol. 4 (5) (2015) 469–487, https://doi.org/10.1002/wdev.189.
[8] Y. Guo, W.T. Pu, Cardiomyocyte maturation: new phase in development, Circ. Res. 126 (8) (2020) 1086–1106, https://doi.org/10.1161/circresaha.119.315862.
[9] S. Lange, N. Pinotsis, I. Agarkova, E. Ehler, The M-band: the underestimated part of the sarcomere, Biochim. Biophys. Acta Mol. Cell Res. 1867 (3) (2020) 118440, https://doi.org/10.1016/j.bbamcr.2019.02.003.
[10] E.P. Lamber, P. Guicheney, N. Pinotsis, The role of the M-band myomesin proteins in muscle integrity and cardiac disease, J. Biomed. Sci. 29 (1) (2022) 18, https://doi.org/10.1186/s12929-022-00801-6.
[11] F. Steiner, K. Weber, D.O. Fürst, Structure and expression of the gene encoding murine M-protein, a sarcomere-specific member of the immunoglobulin superfamily, Genomics 49 (1) (1998) 83–95, https://doi.org/10.1006/geno.1998.5220.
[12] N. Chanthra, T. Abe, M. Miyamoto, K. Sekiguchi, C. Kwon, Y. Hanazono, et al., A novel fluorescent reporter System identifies Laminin-511/521 as potent regulators of cardiomyocyte maturation, Sci. Rep. 10 (1) (2020) 4249, https://doi.org/10.1038/s41598-020-61163-3.
[13] T. Wahyuni, A. Kobayashi, S. Tanaka, Y. Miyake, A. Yamamoto, A. Bahtiar, et al., Maresin-1 induces cardiomyocyte hypertrophy through IGF-1 paracrine pathway, Am. J. Physiol. Cell Physiol. 321 (1) (2021) C82–c93, https://doi.org/10.1152/ajpcell.00568.2020.
[14] A. Miyawaki, Y. Mitsuhara, A. Orimoto, Y. Nakayasu, S. Tsunoda, M. Obana, et al., Moesin is activated in cardiomyocytes in experimental autoimmune myocarditis and mediates cytoskeletal reorganization with protrusion formation, Am. J. Physiol. Heart Circ. Physiol. 311 (2) (2016) H476–H486, https://doi.org/10.1152/ajpheart.00180.2016.
[15] G. Yu, L.G. Wang, Y. Han, Q.Y. He, clusterProfiler: an R package for comparing biological themes among gene clusters, OMICS A J. Integr. Biol. 16 (5) (2012) 284–287, https://doi.org/10.1089/omi.2011.0118.

[16] H. Zhang, L. Pei, Z. Ouyang, H. Wang, X. Chen, K. Jiang, et al., AP-1 activation mediates post-natal cardiomyocyte maturation, Cardiovasc. Res. 119 (2) (2023) 536–550, https://doi.org/10.1093/cvr/cvac088.
[17] Y. Hao, T. Stuart, M.H. Kowalski, S. Choudhary, P. Hoffman, A. Hartman, et al., Dictionary learning for integrative, multimodal and scalable single-cell analysis, Nat. Biotechnol. 42 (2) (2024) 293–304, https://doi.org/10.1038/s41587-023-01767-y.
[18] J. Cao, M. Spielmann, X. Qiu, X. Huang, D.M. Ibrahim, A.J. Hill, et al., The single-cell transcriptional landscape of mammalian organogenesis, Nature 566 (7745) (2019) 496–502, https://doi.org/10.1038/s41586-019-0969-x.
[19] M. Tomimatsu, K. Matsumoto, M. Ashizuka, S. Kumagai, S. Tanaka, T. Nakae, et al., Myeloid cell-specific ablation of Runx2 gene exacerbates post-infarct cardiac remodeling, Sci. Rep. 12 (1) (2022) 16656, https://doi.org/10.1038/s41598-022-21202-7.
[20] Y. Kametani, S. Tanaka, Y. Wada, S. Suzuki, A. Umeda, K. Nishinaka, et al., Yes-associated protein activation potentiates glycogen synthase kinase-3 inhibitor-induced proliferation of neonatal cardiomyocytes and iPS cell-derived cardiomyocytes, J. Cell. Physiol. 237 (5) (2022) 2539–2549, https://doi.org/10.1002/jcp.30724.
[21] S. Suzuki, S. Tanaka, Y. Kametani, A. Umeda, K. Nishinaka, K. Egawa, et al., Runx1 is upregulated by STAT3 and promotes proliferation of neonatal rat cardiomyocytes, Physiol. Rep. 11 (23) (2023) e15872, https://doi.org/10.14814/phy2.15872.
[22] D.A. Prosdocimo, P. Anand, X. Liao, H. Zhu, S. Shelkay, P. Artero-Calderon, et al., Kruppel-like factor 15 is a critical regulator of cardiac lipid metabolism, J. Biol. Chem. 289 (9) (2014) 5914–5924, https://doi.org/10.1074/jbc.M113.531384.
[23] P. Dobrzyn, H. Sampath, A. Dobrzyn, M. Miyazaki, J.M. Ntambi, Loss of stearoyl-CoA desaturase 1 inhibits fatty acid oxidation and increases glucose utilization in the heart, Am. J. Physiol. Endocrinol. Metabol. 294 (2) (2008) E357–E364, https://doi.org/10.1152/ajpendo.00471.2007.
[24] A.N. Paradis, M.S. Gay, L. Zhang, Binucleation of cardiomyocytes: the transition from a proliferative to a terminally differentiated state, Drug Discov. Today 19 (5) (2014) 602–609, https://doi.org/10.1016/j.drudis.2013.10.019.
[25] A.R. Pinto, A. Ilinykh, M.J. Ivey, J.T. Kuwabara, M.L. D'Antoni, R. Debuque, et al., Revisiting cardiac cellular composition, Circ. Res. 118 (3) (2016) 400–409, https://doi.org/10.1161/circresaha.115.307778.
[26] C. Li, X. Rong, J. Qin, S. Wang, An improved two-step method for extraction and purification of primary cardiomyocytes from neonatal mice, J. Pharmacol. Toxicol. Methods 104 (2020) 106887, https://doi.org/10.1016/j.vascn.2020.106887.
[27] X. Yang, S. Li, H. Wang, W. Chen, X. Mou, S. Wang, Expression of coxsackie and adenovirus receptor is correlated with inferior prognosis in liver cancer patients, Oncol. Lett. 17 (2) (2019) 2485–2490, https://doi.org/10.3892/ol.2018.9868.
[28] T. Kashimura, M. Kodama, Y. Hotta, J. Hosoya, K. Yoshida, T. Ozawa, et al., Spatiotemporal changes of coxsackievirus and adenovirus receptor in rat hearts during postnatal development and in cultured cardiomyocytes of neonatal rat, Virchows Arch. : Int. J. Pathol. 444 (3) (2004) 283–292, https://doi.org/10.1007/s00428-003-0925-9.
[29] A.M. Pettinato, F.A. Ladha, J.T. Hinson, The cardiac sarcomere and cell cycle, Curr. Cardiol. Rep. 24 (6) (2022) 623–630, https://doi.org/10.1007/s11886-022-01682-9.
[30] H. Ali, L. Braga, M. Giacca, Cardiac regeneration and remodelling of the cardiomyocyte cytoarchitecture, FEBS J. 287 (3) (2020) 417–438, https://doi.org/10.1111/febs.15146.
[31] D. Montaigne, L. Butruille, B. Staels, PPAR control of metabolism and cardiovascular functions, Nat. Rev. Cardiol. 18 (12) (2021) 809–823, https://doi.org/10.1038/s41569-021-00569-6.
[32] X. Fan, B.G. Hughes, M.A. Ali, W.J. Cho, W. Lopez, R. Schulz, Dynamic alterations to α-Actinin accompanying sarcomere disassembly and reassembly during cardiomyocyte mitosis, PLoS One 10 (6) (2015) e0129176, https://doi.org/10.1371/journal.pone.0129176.
[33] P. Ahuja, E. Perriard, J.C. Perriard, E. Ehler, Sequential myofibrillar breakdown accompanies mitotic division of mammalian cardiomyocytes, J. Cell Sci. 117 (Pt 15) (2004) 3295–3306, https://doi.org/10.1242/jcs.01159.
[34] M.J. Potthoff, M.A. Arnold, J. McAnally, J.A. Richardson, R. Bassel-Duby, E. N. Olson, Regulation of skeletal muscle sarcomere integrity and postnatal muscle function by Mef2c, Mol. Cell Biol. 27 (23) (2007) 8143–8151, https://doi.org/10.1128/mcb.01187-07.
[35] T. Kubin, J. Pöling, S. Kostin, P. Gajawada, S. Hein, W. Rees, et al., Oncostatin M is a major mediator of cardiomyocyte dedifferentiation and remodeling, Cell Stem Cell 9 (5) (2011) 420–432, https://doi.org/10.1016/j.stem.2011.08.013.
[36] A. Beisaw, C. Kuenne, S. Guenther, J. Dallmann, C.C. Wu, M. Bentsen, et al., AP-1 contributes to chromatin accessibility to promote sarcomere disassembly and cardiomyocyte protrusion during zebrafish heart regeneration, Circ. Res. 126 (12) (2020) 1760–1778, https://doi.org/10.1161/circresaha.119.316167.
[37] S. Ikeda, W. Mizushima, S. Sciarretta, M. Abdellatif, P. Zhai, R. Mukai, et al., Hippo deficiency leads to cardiac dysfunction accompanied by cardiomyocyte dedifferentiation during pressure overload, Circ. Res. 124 (2) (2019) 292–305, https://doi.org/10.1161/circresaha.118.314048.
[38] M. Yu, K. Thorner, S. Parameswaran, W. Wei, C. Yu, X. Lin, et al., The unique functions of Runx1 in skeletal muscle maintenance and regeneration are facilitated by an ETS interaction domain, Development (Cambridge, England) 151 (24) (2024), https://doi.org/10.1242/dev.202556.
[39] K.B. Umansky, Y. Gruenbaum-Cohen, M. Tsoory, E. Feldmesser, D. Goldenberg, O. Brenner, et al., Runx1 transcription factor is required for myoblasts proliferation during muscle regeneration, PLoS Genet. 11 (8) (2015) e1005457, https://doi.org/10.1371/journal.pgen.1005457.
[40] R. Agarwal, H. Wakimoto, J.A. Paulo, Q. Zhang, D. Reichart, C. Toepfer, et al., Pathogenesis of cardiomyopathy caused by variants in ALPK3, an essential pseudokinase in the cardiomyocyte nucleus and sarcomere, Circulation 146 (22) (2022) 1674–1693, https://doi.org/10.1161/circulationaha.122.059688.
[41] L. Han, S. Choudhury, J.D. Mich-Basso, N. Ammanamanchi, B. Ganapathy, S. Suresh, et al., Lamin B2 levels regulate polyploidization of cardiomyocyte nuclei and myocardial regeneration, Dev. Cell 53 (1) (2020) 42–59.e11, https://doi.org/10.1016/j.devcel.2020.01.030.